NJC

Accepted Manuscript

Volume 40 | Number 1 | January 2016 | Pages 1–846

NJC

New Journal of Chemistry
www.rsc.org/njc

A journal for new directions in chemistry

ISSN 1144-0546

ROYAL SOCIETY OF CHEMISTRY

PAPER
Jason B. Benedict et al
The role of atropisomers on the photo-reactivity and fatigue of diarylethene-based metal–organic frameworks

cnrs

This is an Accepted Manuscript, which has been through the Royal Society of Chemistry peer review process and has been accepted for publication.

Accepted Manuscripts are published online shortly after acceptance, before technical editing, formatting and proof reading. Using this free service, authors can make their results available to the community, in citable form, before we publish the edited article. We will replace this Accepted Manuscript with the edited and formatted Advance Article as soon as it is available.

You can find more information about Accepted Manuscripts in the author guidelines.

ROYAL SOCIETY OF CHEMISTRY

rsc.li/njc

Crystal Structure, Hirshfeld Surface Analysis, Spectroscopic and Biological Studies on Sulfamethazine and Sulfaquinoxaline Ternary Complexes with 2,2'-Biquinoline.

C. Villa-Pérez[1]; J.F. Cadavid-Vargas[1]; A. L. Di Virgilio[1]; G. Echeverría[2]; G.E. Camí[3] and D.B. Soria[1].

[1]CEQUINOR, CONICET, CCT La Plata, Departamento de Química, Facultad de Ciencias Exactas, Universidad Nacional de la Plata, 1900, La Plata, Argentina. soria@quimica.unlp.edu.ar.

[2]IFLP, CONICET, CCT La Plata, Departamento de Física, Facultad de Ciencias Exactas, Universidad Nacional de La Plata, 1900, La Plata, Argentina.

[3]Química General e Inorgánica, Facultad de Ciencias Bioquímicas y Farmacéuticas, Universidad Nacional de Rosario, 2000, Rosario, Argentina.

ABSTRACT

Three ternary complexes of sulfaquinoxaline (SQO - 4-Amino-N-2-quinoxalinylbenzenesulfonamide) or sulfamethazine (SMT - 4-Amino-N-(4,6-dimethylpyrimidin-2-yl)-benzenesulfonamide) with Cu(II) or Ni(II) and 2, 2'-biquinoline (BQ) as auxiliary ligand have been studied. Their structures have been determined by single-crystal X-ray crystallography as $Ni(SQO)_2(BQ)\cdot2H_2O$ (**I**), $Cu(SQO)(BQ)Cl\cdot CH_3OH$ (**II**) and $Cu(SMT)(BQ)Cl$ (**III**). Compounds **I** and **II** crystallize in the triclinic space group P-1 while complex **III** in the monoclinic $P2_1/c$ space group. The crystal lattice of all complexes is stabilized by the presence of diverse intermolecular interactions as verified by Hirshfeld surface analysis. Besides, electronic spectroscopies have also been used to characterize the compounds. The thermal behavior of the complexes was investigated by thermogravimetric and differential thermal analyses. Furthermore, the cytotoxic effect of the compounds has been tested against A549 (lung cancer) and MG-63 (human osteosarcoma) cell lines using the MTT methodology.

Keywords – Sulfaquinoxaline; Sulfamethazine; X-ray structure; Hirshfeld surface calculations; Intermolecular interactions; Cytotoxicity.

INTRODUCTION

Sulfonamide compounds are recognized for their biological properties [1–6] and their different coordination modes [5]. A wide variety of metal complexes with N-sulfonamides derivatives has also been studied for their polymer stabilization capacity [2], magnetic behavior [7–10], electrochemical properties [8,9,11] and luminescent emission [12,13]. Some complexes with sulfaquinoxaline (SQO) or sulfamethazine (SMT) as ligands (see Scheme 1) have been reported as effective chemotherapeutic

agents. In the case of SQO, a polymeric Cd(II) complex [12] and some monomeric ternary Co(II) [3] and Zn(II) [13] complexes have been described. On the other hand, some sulfamethazine complexes have been described as monomeric, dimeric and polymeric M(II) derivatives [5,9–11,14–16].

The understanding of noncovalent interactions (e.g., H-bonding, π-forces) results useful in the design of new compounds in a wide range of fields (e.g. materials, pharmaceuticals). In the case of sulfonamide metal complexes, inter and intramolecular hydrogen bonding, $\pi\cdots\pi$, and C—H$\cdots\pi$ interactions have a great influence on the crystal lattice stabilization [1,3,5,8,17]. The Hirshfeld surface analysis is a powerful tool for visualizing and quantifying the contribution of such intermolecular interactions to supramolecular assemblies [18–20].

As part of our ongoing research on the study of the structural and physicochemical properties of sulfonamides metal complexes [3,7,21,22], we have previously reported the study in different models of biological systems in a ternary cobalt complex with sulfaquinoxaline and 2,2`-Bypirimidine as ligand[3]. Our goal herein is to extend these studies to other auxiliary ligands and metals with eventual biological properties. We report the synthesis of three ternary complexes of Ni(II) (**I**) and Cu(II) (**II** and **III**), using sulfaquinoxaline or sulfamethazine as primary ligands and 2,2'-biquinoline as a coligand. They have been characterized by thermogravimetry, and by single-crystal X-ray diffraction, Fourier Transform Infrared, UV-Vis and fluorescence spectroscopies. Hirshfeld surface analysis has been applied to visualize the presence of different intermolecular interactions. Furthermore, MTT assays have been performed for the complexes, the free ligands and the corresponding M(II) salts to explore their cytotoxic capacity.
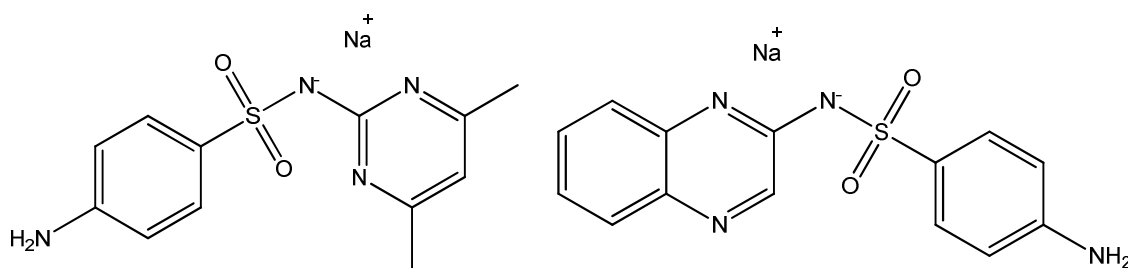
Scheme 1. Structural formulae for sulfamethazine (SMT) and sulfaquinoxaline (SQO) sodium salts.

1. EXPERIMENTAL

1.1. *Synthesis of the complexes*

All the reagents were obtained from Sigma Chemical Company (St. Louis, MO, USA) and used without further purification.

Synthesis of Ni(SQO)₂BQ·2H₂O (**I**):

A hot methanolic solution containing 2,2'-biquinoline (0.2 mmol, 51.3 mg) and NaSQO (0.4 mmol, 128.9 mg - sulfaquinoxaline sodium salt) was added dropwise under continuous stirring to a methanolic solution of $NiCl_2 \cdot 6H_2O$ (0.2 mmol, 47.5 mg). A lime green powder was obtained, centrifuged and washed several times with methanol. After a few days, well developed green crystals were separated from the mother liquor and subjected to X-ray diffraction studies. Both crystals and powder were identical as shown by their FTIR spectra. The same product was obtained using a different molar ratio (e.g. 1:1:1). The elemental analysis (AE [%]) for $NiC_{46}H_{34}N_{10}O_4S_2 \cdot 2H_2O$ gave the following results: Exp. (calc.): C: 58.38 (58.18); H: 4.17 (4.03); N: 14.79 (14.75); S: 6.61 (6.75) %. FTIR data (cm^{-1}): v_{as} (NH$_2$) 3696, v_s (NH$_2$) 3614, v (C=N and C=C) 1633 – 1492, v_{as} (SO$_2$) 1349, v_s (SO$_2$) 1092 cm^{-1}. Yield: 161.2 mg (84.9 %).

Synthesis of Cu(L)(BQ)Cl (L = SQO **(II)** or SMT **(III)**):

For the compound **II,** a methanolic solution of $CuCl_2 \cdot 2H_2O$ (0.4 mmol, 68.2 mg) was added dropwise to a hot methanolic solution including 2,2'-biquinoline (0.4 mmol, 102.5 mg) and NaSQO salt (0.4 mmol, 128.9 mg). Complex **III** was prepared following the same synthesis procedure, but using NaSMT (0.4 mmol, 120.1 mg - sulfamethazine sodium salt) instead of NaSQO. The reactions were refluxed for 2 h affording purple solutions which were filtered. After a few days, brownish crystals suitable for X-ray analysis were obtained. **II:** AE (%) for $CuC_{32}H_{23}N_6O_2SCl \cdot CH_3OH$: Exp. (calc.): C: 57.21 (57.72); H: 3.76 (3.96); N: 12.79 (12.24); S: 4.82 (4.67) %. FTIR data (cm^{-1}): v_{as} (NH$_2$) 3696, v_s (NH$_2$) 3358 v (C=N and C=C) 1630 – 1493, v_{as} (SO$_2$) 1351, v_s (SO$_2$) 1088. Yield: 133.1 mg (48.5%). **III**: AE (%) for $CuC_{30}H_{25}N_6O_2SCl$: Exp. (calc.): C: 56.58 (56.96); H: 3.87 (3.98); N: 13.67 (13.28); S: 5.03 (5.07) %. FTIR: v_{as} (NH$_2$) 3501, v_s (NH$_2$) 3455, v (C=N and C=C) 1630 – 1491, v_{as} (SO$_2$) 1213, v_s (SO$_2$) 1083. Yield: 164.0 mg (64.3%).

1.2. Instrumentation

FTIR spectra were recorded using a Bruker EQUINOX 55 FTIR (Billerica, MA, USA) spectrophotometer using the KBr pellet technique with a resolution of 4 cm^{-1} in the 4000 – 400 cm^{-1} spectral range. The UV-Vis spectra were recorded in DMSO solution in 10 mm quartz cuvettes, and the diffuse reflectance UV-Vis (V-DR) spectra were measured by using BaSO$_4$ as a reference and employing a Shimadzu UV-2600 Spectrophotometer (Kyoto, Japan). The fluorescence spectra were recorded on a Shimadzu RF-6000 spectrofluorometer in 10 mm quartz cuvette. TG and DT analyses were performed by using Shimadzu TG-50 and DT-50 units from room temperature up to 800 ºC at a heating rate of 5 ºC min^{-1} and oxygen or nitrogen flow of 50 mL min^{-1}.

1.2.1. X-ray data collection and Structure refinement

The data for the complexes were collected on an Agilent Gemini Diffractometer with an EOS CCD detector equipped with a graphite-monochromated Mo Kα (λ = 0.71073 Å) and Cu Kα (λ = 1.54184 Å) radiation. X-ray diffraction intensities were collected (ω scans with θ and κ-offsets), integrated and scaled with CRYSALISPRO [23] suite of programs. The unit cell parameters were obtained by least-squares refinement (based on the angular settings for all collected reflections with intensities larger than seven times the standard deviation of measurement errors). Data were corrected empirically for absorption employing the multi-scan method implemented in CRYSALISPRO (Agilent Technologies Ltd., Yarnton, Oxfordshire, UK). The structures were solved by direct methods with SHELXS-97 (Göttingen, Lower Saxony, Germany) [24] and the molecular models refined by the full-matrix least-squares procedure on F² with SHELXL-97 [25,26]. All hydrogen atoms were located stereochemically except for those of the amino groups which were positioned from a difference Fourier map and refined riding on the bound atom with isotropic displacement parameters. Crystal data and refinement results are summarized in Table 1. CIF files with details of the crystal structures reported in this paper have been deposited with the Cambridge Crystallographic Data Centre, under deposition numbers CCDC 1560251 - 1560253.

Table 1

Crystal data and structure refinement for the complexes.

Compound	I	II	III
Empiric formula	$NiC_{46}H_{34}N_{10}O_4S_2 \cdot 2H_2O^{(b)}$	$CuC_{32}H_{23}N_6O_2SCl \cdot CH_3OH$	$CuC_{30}H_{25}N_6O_2SCl$
Formula weight	949.68	686.67	632.62
Temperature [K]	293(2)	293(2)	293 (2)
Wavelength [Å]	0.71073 (MoKα)	1.54184 (CuKα)	1.54184 (CuKα)
Crystal system	Triclinic	Triclinic	Monoclinic
Space group	P-1	P-1	$P2_1/c$
Unit Cell dimensions [Å, °]			
a	11.9807(9)	10.0919(9)	10.0254(7)
b	12.207(1)	10.1848(6)	16.525(1)
c	17.381(1)	17.013(1)	17.0838(8)
α	84.14(1)	81.383(5)	
β	73.892(9)	75.712(7)	95.697(6)
γ	67.836(9)	63.935(7)	
Volume [Å³]	2261.7(4)	1520.5(2)	2816.4(3)
Z, Density (calculated) [g cm⁻³]	2, 1.389	2, 1.4976	4, 1.492
Absorption coefficient [mm⁻¹]	2.843	2.894	2.988
F(000)	916.0	706	1300
Crystal Size [mm]	0.095 × 0.145 × 0.204	0.019 × 0.108 × 0.216	0.026 × 0.072 × 0.263
θ range for data collection [º]	3.029 - 29.543	4.839 - 72.407	4.43 - 72.76
Index ranges	-15 ≤ h ≤ 16	-12 ≤ h ≤ 12	-12 ≤ h ≤ 10
	-11 ≤ k ≤ 16	-10 ≤ k ≤ 12	-20 ≤ k ≤ 20
	-22 ≤ l ≤ 23	-20 ≤ l ≤ 19	-14 ≤ l ≤ 20
Reflections collected/Unique	20532 / 10504	11418 / 5930	21058 / 5529

	[R(int) = 0.0575]	[R(int) =0.0423]	[R(int) =0.0909]
Completeness to θ	0.997 (θ = 25.242º)	0.982 (θ = 67.684º)	0.999 (θ = 67.684°)
Absorption correction	Semi-empirical	Semi-empirical	Semi-empirical
Max. and min. transmission	1.00000 and 0.83504	1.00000 and 0.92779	1.00000 and 0.87984
Refinement method	FMLS[(c)] on F^2	FMLS[(c)] on F^2	FMLS[(c)] on F^2
Data/restraints/parameters	10504 / 6 / 597	5930 / 0 / 408	5529 / 0 / 370
Goodness-of-fit on F2	1.028	1.028	1.023
Final R indices [I > 2σ(I)][a]	R1= 0.0685 wR2=0.1715	R1= 0.0446 wR2=0.1054	R1= 0.0640 wR2=0.1612
R indices (all data)[a]	R1= 0.1435 wR2=0.2210	R1= 0.0635 wR2=0.1198	R1= 0.1051 wR2=0.1912
Largest diff. peak and hole [e.Å⁻³]	0.879 and -0.401	0.420 and -0.303	1.070 and -0.358

[a]R1=$\Sigma||F_o|-|F_c||/\Sigma|F_o|$, wR2= $[\Sigma w(|F_o|^2-|F_c|^2)^2/\Sigma w(|F_o|^2)^2]^{1/2}$; [b] One hydration water molecule is disorder on two general positions, [c] Full-matrix least-squares.

1.2.2. Computational details

The quantum computational study of the complexes was performed using the density functional theory (DFT) method implemented in the Gaussian 03 package [27]. The three complexes were subjected to unrestrained energy minimizations using the B3LYP [28] functional with the 6-31+G** basis set [29] for non-metal atoms and the Los Alamos effective core potentials LANL2DZ [30–32] for the metal. Based on the second derivatives, the vibrational modes have been calculated, and the most relevant of them have been assigned (See synthesis section).

1.2.3. Hirshfeld surface computational method.

Hirshfeld surfaces and their respective 2D fingerprint plots for all the complexes were calculated with the aid of the CRYSTALEXPLORER 3.1 software [18–20]. Hirshfeld surfaces and 2D fingerprint plots are useful to quantify the nature of the intermolecular interactions in the crystal lattice. The d_{norm} is a function of distances to the surface from nuclei (atoms) inside (di) and outside (de) the Hirshfeld surface, compared with their respective van der Waals radii. The 3D d_{norm} surfaces are plotted over a fixed color scale of -0.25 au (red) – 0.95 au (blue). The 2D fingerprint plots were displayed in the 0.5 - 2.8 Å range, and including reciprocal contacts. Shape index plots were mapped in the color range -1.0 au (concave) to 1.0 au (convex), and the curvedness in the range of -4.0 au (flat) – 0.4 au (singular).

1.3. Biological Studies

Materials

Tissue culture materials were purchased from Corning (Princeton, NJ, USA) and APBiotech (Buenos Aires, Argentina); Dulbecco's Modified Eagle Medium (DMEM), TrypLE™ from Gibco (Gaithersburg, MD, USA); and fetal bovine serum (FBS) from Internegocios SA (Buenos Aires, Argentina). MTT (3-(4,5-Dimethylthiazol-2-yl)-2,5-Diphenyltetrazolium Bromide) from Invitrogen

Corporation (Buenos Aires, Argentina) and, MG-63 and A549 cell lines were obtained from American Type Culture Collection (ATCC®).

Cell Culture

Cell lines MG-63 (human osteosarcoma) and A549 (human lung carcinoma) were cultured in DMEM, supplemented with 10% FBS, 100 U/mL penicillin and 100 µg/mL streptomycin. They were kept in an incubator with humidified atmosphere and 5 % of CO_2 at 37 °C. The cells were seeded in a T75 flask, and when 80-90% of confluence was reached, they were subcultured using 1 mL TrypLE™ per 75 cm^2. For each experiment, cells were placed on multiwell plates and allowed to grow for 24 hours. Before each experiment, the cellular monolayer was washed with PBS.

The cell viability was determined using the 3-(4,5-dimethylthiazol-2-yl)-2,5-diphenyltetrazolium bromide (MTT) assay, described by Mosmann [33]. Briefly, 25000 cells were seeded in 96 wells plates and allowed to grow for 24 hours. Afterward, the cells were exposed to different concentrations of the complexes and their precursors for another 24 hours. Subsequently, the monolayer was washed with phosphate buffered saline, and the medium was replaced with fresh DMEM supplemented with 0.5 mg/mL of MTT and incubated for 3 hours under normal culture conditions. This assay is based on the ability of the cells to reduce the MTT to an insoluble purple formazan dye, which was extracted with DMSO (100 µL/well). The absorbance was recorded with a multi-plate reader Multiskan FC (Thermo Scientific) at 570 nm. Each assay was performed at least three times independently. Tukey's and Dunnett's multiple comparisons tests were applied with an alpha value of 0.05, with n=9 and the IC50 was calculated for each compound. The cell viability is shown graphically as the percent of the control value and was calculated according to the following equation.

$$\% \ cell \ viability = \frac{absorbance \ sample \ _{570 \ nm}}{absorbance \ control \ _{570 \ nm}} \ x \ 100$$

2. RESULTS AND DISCUSSION

2.1. Crystal structure analysis

The crystal structure of complexes **I, II** and **III** consists of one neutral Ni(SQO)$_2$BQ, Cu(SQO)(BQ)Cl and (Cu(SMT)(BQ)Cl) unit, respectively. In addition, complex **I** has two hydration water molecules, and one of them is structurally disordered on two general crystallography sites (O1w or O3w). Complex **II** crystallizes with a methanol molecule while **III** with none solvation molecules.

Both, **I** and **II** crystallize in the triclinic P-1 space group with two molecules per unit cell, while **III**, crystallizes in the monoclinic P2$_1$/c space group with four unities per unit cell. In **I**, the Ni(II) atom is coordinated by one biquinoline and two sulfaquinoxaline molecules completing a NiN$_6$ distorted octahedron. On the other hand, in both Cu(II) complexes (**II** and **III**), the metallic center is surrounded by four Nitrogen atoms and one Chlorine atom, forming a CuN$_4$Cl distorted square pyramid. In all complexes, SQO, SMT and biquinoline act as bis-chelating ligands.

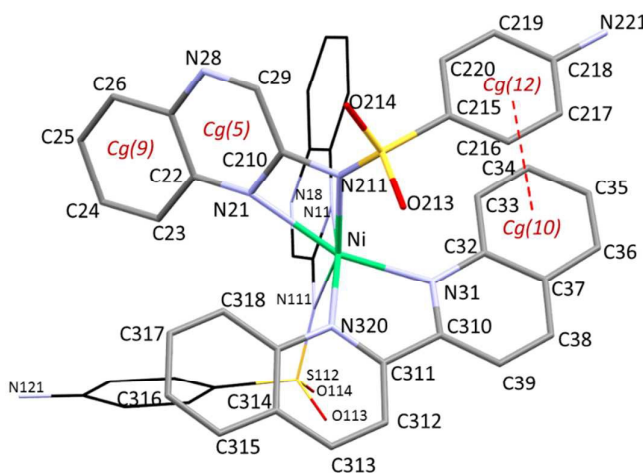The coordination spheres of the complexes and the used labels are illustrated in Figures 1, 2 and 3.

Figure 1. Coordination sphere of the complex **I** with the used labels; H-atoms, some labels and water molecules were omitted for simplicity. The intramolecular π···π stacking Cg(10) ··· Cg(12) is denoted with a red dashed line.
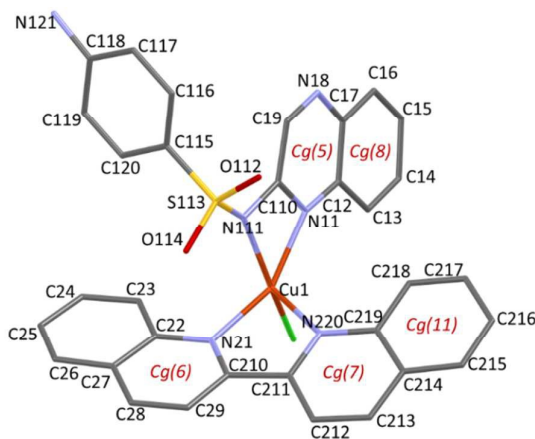

Figure 2. Complex **II** with the used labels, the H-atoms and solvent molecules were omitted for the sake of clarity.
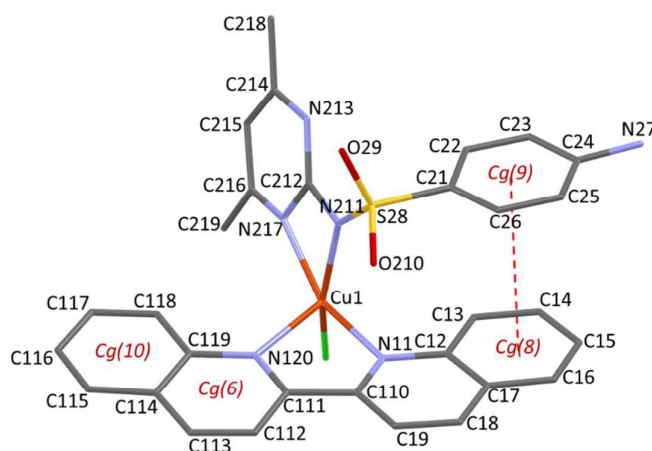
7

Figure 3. Complex **III** with the used labels, the H-atoms were omitted for the sake of clarity. The intramolecular π···π stacking Cg(8) ···Cg(9) is denoted with a red dashed line.

The degree of distortion of the NiN_6 and CuN_4Cl coordination polyhedra with respect to ideal six and five vertex polyhedra was estimated using the SHAPE software [34] which considers the continuous shape measure theory. In **I**, values of 5.051 for the octahedron (OC-6) and 12.956 for the trigonal prism (TPR-6), indicate that the polyhedron around the Ni(II) center is better described by the octahedral geometry. For **II** and **III,** the coordination sphere is found between the vacant octahedron (vOC-5) and the square pyramid (SPY-5) geometries with values of 4.041 and 3.451 for **II** and 4.148 and 3.373 for **III,** respectively. These values suggest that both complexes are closer in shape to the square pyramid geometry. (See tables S1 and S2**;** see the Electronic Supporting Information, ESI). The geometrical parameters, obtained from the X-ray diffraction experiments using the PLATON software [35] together with the computed values [B3LYP/6-31+G**] are listed in tables S3-S5 in the ESI, and the correlation between the calculated and the experimental data is presented in Figure S1.

The calculated geometrical parameters are in good agreement with their experimental counterparts as can be observed in the slopes of the correlation plots (See Fig. S1) and the RMS values: 0.668, 0.402 and 0.156 Å for **I**, **II** and **III**, respectively**.**

2.2. Hirshfeld surface analysis

By using the crystallographic data, Hirshfeld surface analysis was performed to investigate the nature and quantitative contributions of intermolecular interactions to the supramolecular assembly of the complexes which are stabilized by several kinds of interactions. The Hydrogen bonding and π-π interactions for the three complexes are summarized in Tables **2** and **3**, respectively.

Table 2. Hydrogen bonding for compounds **I, II** and **III** [Å, º].

	D—H⋯A	D—H	H⋯A	D⋯A	∠ D—H⋯A	Label (Fig. 3)
I	N_{121}—H_{123}⋯N_{18}ⁱ	0.88	2.17	3.0469(4)	172	1
	O_{1w}—H_{12w}⋯O_{214}^{vi}	0.85	2.25	3.0361(3)	154	2
	O_{3w}—H_{31w}⋯O_{214}^{vi}	0.85	2.11	2.9328(3)	163	3
	N_{121}—H_{122}⋯O_{2w}^{vii}	0.86	2.15	2.9709(3)	157	4
	O_{2w}—H_{22w}⋯N_{121}	0.85	2.38	3.2187(4)	171	5
	O_{2w}—H_{21w}⋯N_{28}^{vi}	0.85	2.22	2.8451(3)	130	6
	O_{3w}—H_{32w}⋯O_{114}ⁱ	0.85	2.19	3.0331(3)	169	7
	C_{19}—H_{19}⋯O_{3w}ⁱ	0.93	2.57	3.3981(4)	148	8
	N_{221}—H_{223}⋯O_{1w}^{viii}	0.86	2.21	3.0573(4)	167	9
	C_{219}—H_{219}⋯O_{113}^{ix}	0.93	2.56	3.3400(4)	142	10
	C_{35}—H_{35}⋯O_{113}^x	0.93	2.71	3.5268(4)	147	12
II	N_{121}—H_{211}⋯N_{18}ⁱ	0.98	2.26	3.1658(3)	154	1
	C_{215}—H_{215}⋯O_{114}ⁱⁱ	0.93	2.50	3.3743(3)	156	2
	C_{16}—H_{16}⋯O_{31}^{MeOH}	0.93	2.46	3.3740(3)	166	3
	C_{213}—H_{213}⋯O_{112}ⁱⁱ	0.93	2.70	3.5653(3)	156	5
	C_{217}—H_{217}⋯C_{120}ⁱⁱⁱ	0.93	2.85	3.7360(5)	160	6
	C_{216}—H_{216}⋯O_{114}^{iv}	0.93	2.66	3.3254(3)	130	7
	C_{29}—H_{29}⋯Cl_3^v	0.93	2.81	3.5122(3)	133	8
	C_{15}—H_{15}⋯C_{120}^{vi}	0.93	2.80	3.6470(4)	152	9
	O_{31}^{MeOH}—H_{31}^{MeOH}⋯Cl_3^{vi}	0.82	2.51	3.2712(3)	154	10
III	N_{27}—H_{27A}⋯O_{210}^{xi}	0.86	2.53	2.9421(2)	110	1
	C_{18}—H_{18}⋯O_{29}^{xiii}	0.93	2.44	3.3306(2)	157	2
	C_{15}—H_{15}⋯O_{29}^{xiv}	0.93	2.60	3.4485(2)	151	3
	C_{19}—H_{19}⋯C_{22}^{xiii}	0.93	2.90	3.5608(2)	129	4
	C_{218}—H_{21C}⋯Cl_2^{xii}	0.93	2.80	3.7089(3)	158	6

Symmetry operations: (i) -x, 1-y, 1-z; (ii) –x, -y, 2-z; (iii) x, -1+y, z; (iv) x, 1+y, z; (v) 1-x, -y, 2-z; (vi) 1-x, -y, 1-z; (vii) –x, -y, 1-z; (viii) 1+x, y, -1+z; (ix) 1+x, y, z; (x) 1-x, 1-y, -z, (xi) x, ½-y, -½+z; (xii) 1-x, -½+y, ½-z; (xiii) -x, ½+y, ½-z; (xiv) x, ½ -y, ½+z; (xvi) -x, - ½+y, ½-z; (xvi) 1-x, 1-y, 1-z.

In compounds **I** and **II** centrosymmetric $R_2^2(22)$ motifs are formed by the establishment of N—H⋯N hydrogen bonds (Table 2 and Figures 4 and S2). Figure 5 shows the d_{norm} surfaces of the complexes with the strong N—H⋯N hydrogen bonds as two deep-red zones labeled as 1.
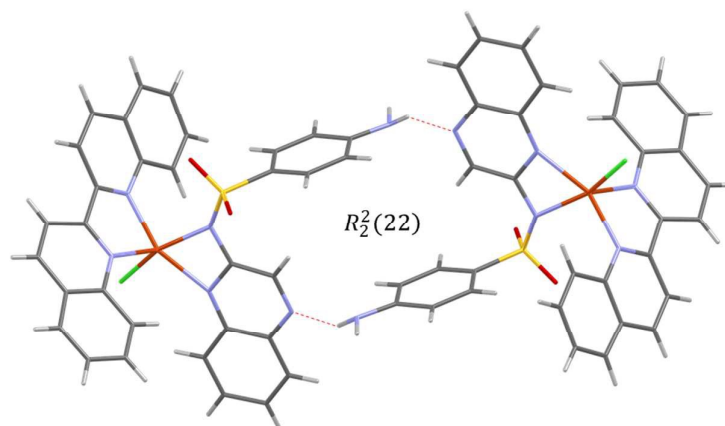
Figure 4. $R_2^2(22)$ motifs formed between complex **II** unities, the intermolecular interactions are depicted as red dashed lines. Solvation molecules were omitted for simplicity.
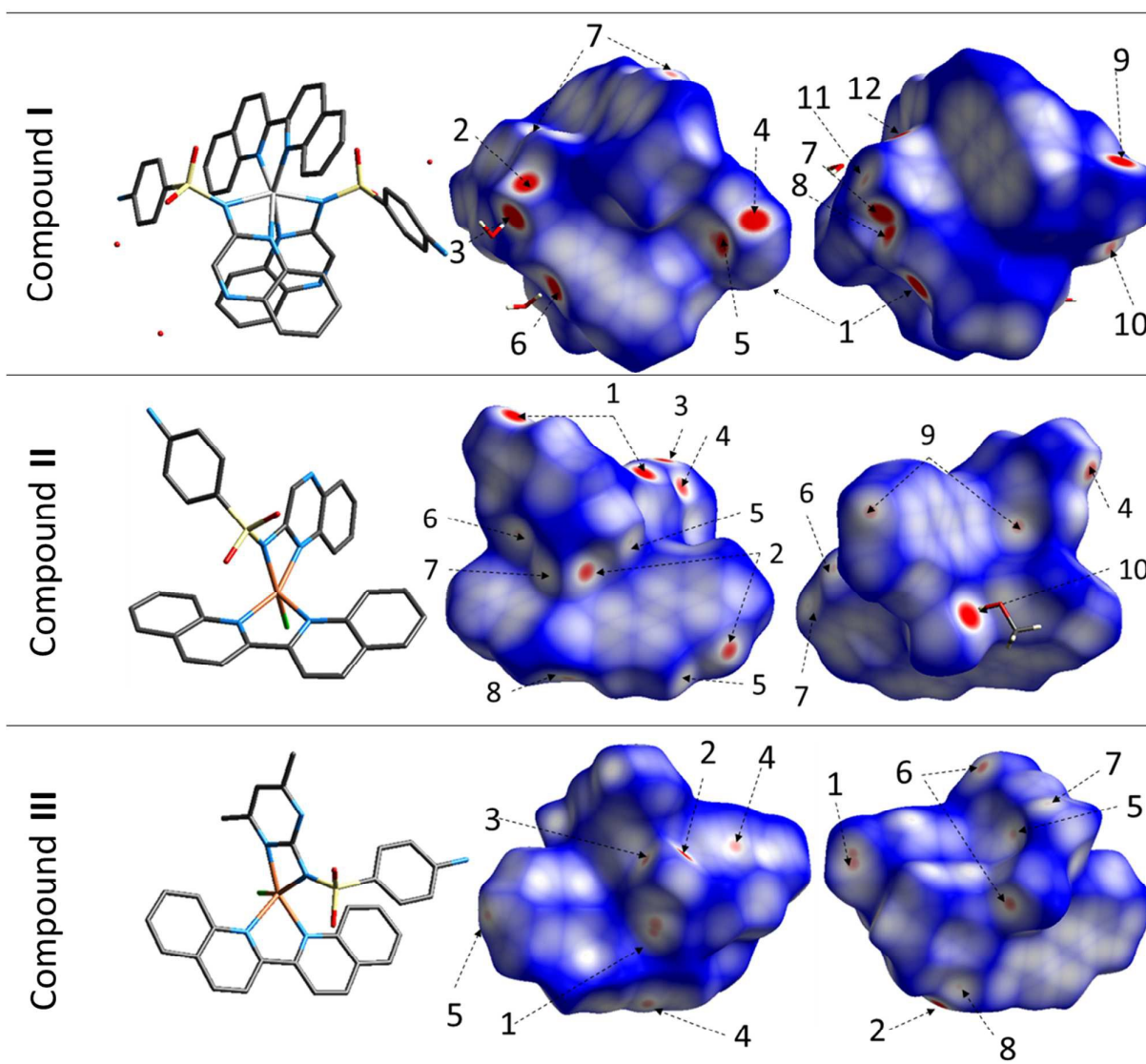
Figure 5. Views of two orientations in the Hirshfeld surfaces for the three complexes. The first column shows the molecule orientation in the surface of column 2. The third column shows the surface rotated by 180° around the vertical axis of the plot; H-atoms are omitted for simplicity; numbered arrows are described either in Table 2 or the text.

Another important feature of the supramolecular structure is the effect of the solvate molecules. In **I** the water molecules are involved in several strong hydrogen bonding interactions (labeled as 3 and 6 in Figure 5). The disordered water molecule interacts with an SO_2 sulfonamide group in a non-conventional intermolecular $O1w\cdots O114$ at a 2.93(1) Å distance (labeled as 11 in Figure 5). Even

though this type of interactions is not very common, they play an important role in some supramolecular assemblies [36].

In **II**, the methanol molecule is involved in a strong O—H···Cl hydrogen bond interaction observed in the d_{norm} surface as an intense red spot (10) near the H_{31}^{MeOH} proximity. In **III,** the relative contribution of O^{SO_2}···H interactions is lower than in **I** or **II** compounds due to the absence of solvation molecules (see Table 2). In all the complexes C—H···O interactions are also present (labeled as 8, 10 and 12, for **I**; 2, 3, 5 and 7, for **II**; 2 and 3, for **III**; see Figure 5). These interactions are established with both H-atoms from solvation molecules as well as with those belonging to the ligands. Furthermore, in **II** and **III**, non-classical C—H···C interactions (labels 6 and 9, for **II**; and 4, 5 and 8 for **III**) and C—H···Cl hydrogen interactions (labeled as 8 and 10, for **II**; and 6, for **III**) are observed.

Figure 6 shows the fingerprint plots and the relative contributions of the main intermolecular contacts. The H···H interactions are the shortest contacts in **I**, and they are depicted as a sharp, centered spike (de + di ~ 1.8 Å). Besides, the C···H intermolecular interactions belong to the C···H—C contacts (de + di ~ 3.9 and 4.4 Å). Furthermore, the N···H interactions correspond with both N···H—N and N···H—Ow contacts (de + di ~ 4.0 Å). Additionally, the O···H interactions are asymmetrically depicted as three sharp spikes (de + di ~ 2.0 and 2.45 Å). This fact could be explained considering the presence of different kinds of intermolecular interactions O···H—X (X = N, C or O. See Table 2). Finally, the C···C interactions are due to π···π contacts between the biquinoline rings (de + di ~ 3.6 Å).

For complex **II,** the shortest distance is associated with N···H contacts. The fingerprint shows two sharp spikes near a (de + di) sum of 1.75 Å corresponding to the N—H···N interactions observed in the $R_2^2(22)$ dimers, previously discussed. Dihydrogen bond interactions (H···H) are depicted as a centered spike with a de + di sum of ~ 2.4 Å. The O···H interaction between the methanol molecule and the complex is observed as two sharp spikes (de + di ~ 2.8 Å). Besides, the π···π interactions are observed as a light blue area on the diagonal at approximately 1.8 Å. These interactions are due to the C···C contacts (quinoxalinyl - biquinoline). The C···H contacts are depicted as two pairs of spikes indicating two different C···H interactions (de + di ~ 2.7 and 3.4 Å). Lastly, the Cl···H contacts are observed as two symmetrical spikes that belong to the Cl···H—C interactions (de + di ~ 2.6 Å).

The 2D fingerprint of **III** shows that the H···H interactions are the shortest (de + di ~ 2.2 Å) and the O···H contacts are depicted as two symmetrical spikes at de + di ~ 2.3 Å. In regard to the N···H interactions, the fingerprint shows two broad symmetrical zones centered at nearly de + di ~ 3.4 Å.

The C···H contacts are characterized by a 3 Å de + di distance, slightly shorter than that of the N···H interactions. Furthermore, the C···C interactions are shown as a light blue zone at de + di ~ 3.6 Å due to the interaction between two adjacent biquinoline. Finally, the Cl···H interactions are represented as two sharp spikes located at de + di ~ 2.7 Å.

Quantitative examination of 2D fingerprint plots revealed that H···H interactions play the most important contribution to the total Hirshfeld Surface with a contribution of 44.2, 41.0 and 44.5 %, for **I**, **II** and **III**, respectively (see Fig. 6). These interactions can also be observed in the d_{norm} 3D plot (Figure 5), for example, H212···H16 in compound **II** (label 4) and H21B···H21F in **III** (label 7).

The contribution of C···H interactions to the lattice is similar for the three compounds; the same fact occurs for the N···H interactions. However, in compound **I** the quantitative contribution of the O···H interactions is higher than in **II** and **III.** This fact can be explained due to the different solvation in the three complexes.

In compound **II** the contribution of the C···C interactions is higher than in **I** and **III** due to the difference in the π···π interactions (see Figures 6 and 7). Also, there are some other interactions with a minor quantitative contribution to the supramolecular assemblies (e.g. O···O, Cl···O; < 3.2 %).

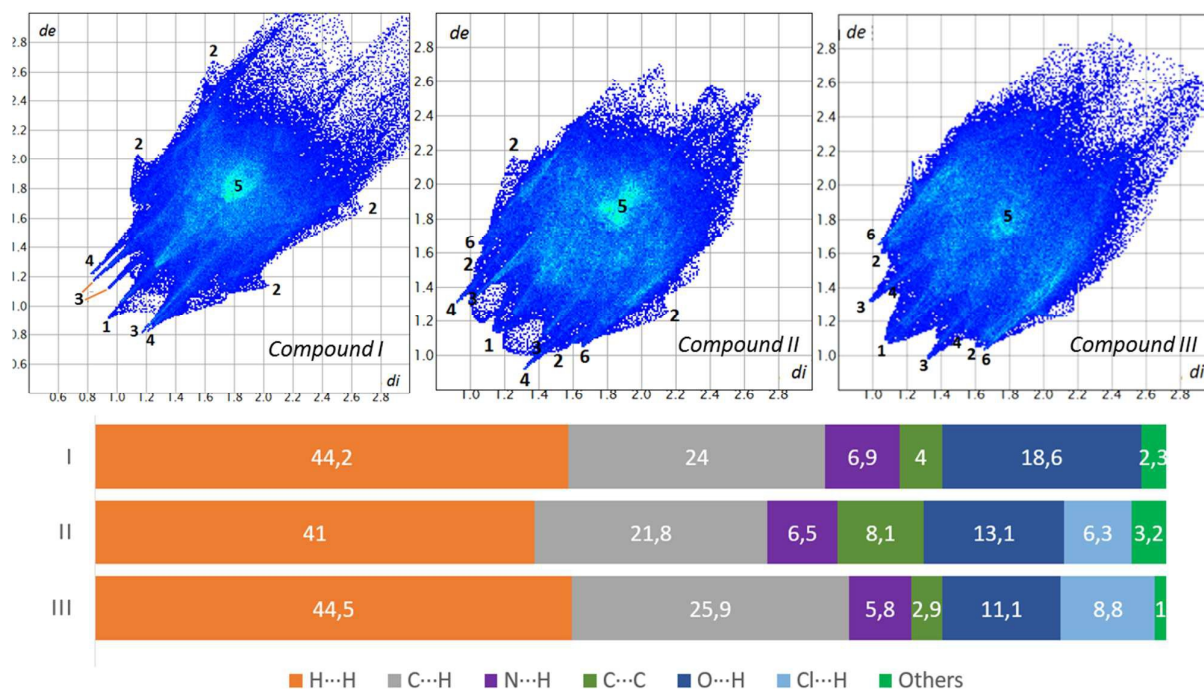**Figure 6.** Top: 2D Fingerprint plots for the compounds. Close contacts are labeled as: (1) H···H, (2) C···H, (3) O···H, (4) N···H, (5) C···C and (6) Cl···H. Bottom: Relative contributions of the

intermolecular interactions to the Hirshfeld surface for the compounds [%].

In compounds, **I** and **III** intramolecular $\pi\cdots\pi$ interactions between the biquinoline and the aniline moiety of one sulfonamide ligand are observed (**I**: Cg(10) $\cdots$ Cg(12), **III**: Cg(8) $\cdots$ Cg(9) Å; see Figures 1 and 3). Furthermore, in all the complexes a significant contribution of intermolecular $\pi\cdots\pi$ interactions is observed. In **I** and **II**, the quinoxalinyl segments of adjacent molecules interact at different distances (Cg(5) $\cdots$ Cg(9)^{vi} and Cg(5) $\cdots$ Cg(8)^{vi}) (See Figs. 1 and 2). In compound **II** two different BQ$\cdots$BQ interactions are observed (Cg(6)$\cdots$Cg(7)^{v} and Cg(7)$\cdots$Cg(11)^{ii}) and in **III** (Cg(6) $\cdots$ Cg(6)^{xvi} and Cg(6) $\cdots$ Cg(10)^{xvi}) (See Fig. 3). The geometrical parameters of these π-stacking interactions are presented in Table 3. These $\pi \cdots \pi$ interactions can be visualized in the complexes Shape-index and curvedness plots (Figure 7). This kind of interaction is evidenced by the presence of a triangles pattern and a high planarity zone in the shape-index and curvedness surface, respectively.

Table 3. Geometrical parameters [Å, º] for the π-stacking interactions in **I**, **II** and **III**.

Rings I-J	Rc[a]	R1v[b]	R2v[c]	α[d]	β[e]	γ[f]
Compound **I**						
Cg (5) $\cdots$ Cg (9) ^{vi}	4.0812(5)	3.4003	3.3818	1	34.0	33.6
Cg (10) $\cdots$ Cg (12) $^{intra.}$	3.7362(4)	3.3336	3.3046	2	27.8	26.8
Compound **II**						
Cg (5) $\cdots$ Cg (8) ^{vi}	3.7370(3)	3.4567	3.5309	3	19.1	22.3
Cg (6) $\cdots$ Cg (7) ^{v}	4.0651(4)	3.3805	3.8703	18	17.8	33.7
Cg (7) $\cdots$ Cg (11) ^{ii}	3.9069(3)	3.5626	3.5275	2	25.5	24.2
Compound **III**						
Cg (8) $\cdots$ Cg (9) $^{intra.}$	3.8357(3)	3.6280	3.5940	3	20.4	18.9
Cg (6) $\cdots$ Cg (6) ^{xvi}	3.5046(2)	3.3724	3.3724	0	15.8	15.8
Cg (6) $\cdots$ Cg (10) ^{xvi}	3.8391(3)	3.3788	3.3705	0	28.6	28.3

[a]Centroid distance between ring I and ring J. [b]Vertical distance from ring centroid I to ring J. [c]Vertical distance from ring centroid J to ring I. [d]Dihedral angle between mean planes I and J. [e]Angle between centroid vector Cg(I) $\cdots$ Cg(J) and the normal to the plane (I). [f]The angle between the centroid vector Cg(I) $\cdots$ Cg(J) and the normal to the plane (J). Roman superscripts denote symmetry operations (see Table 2).
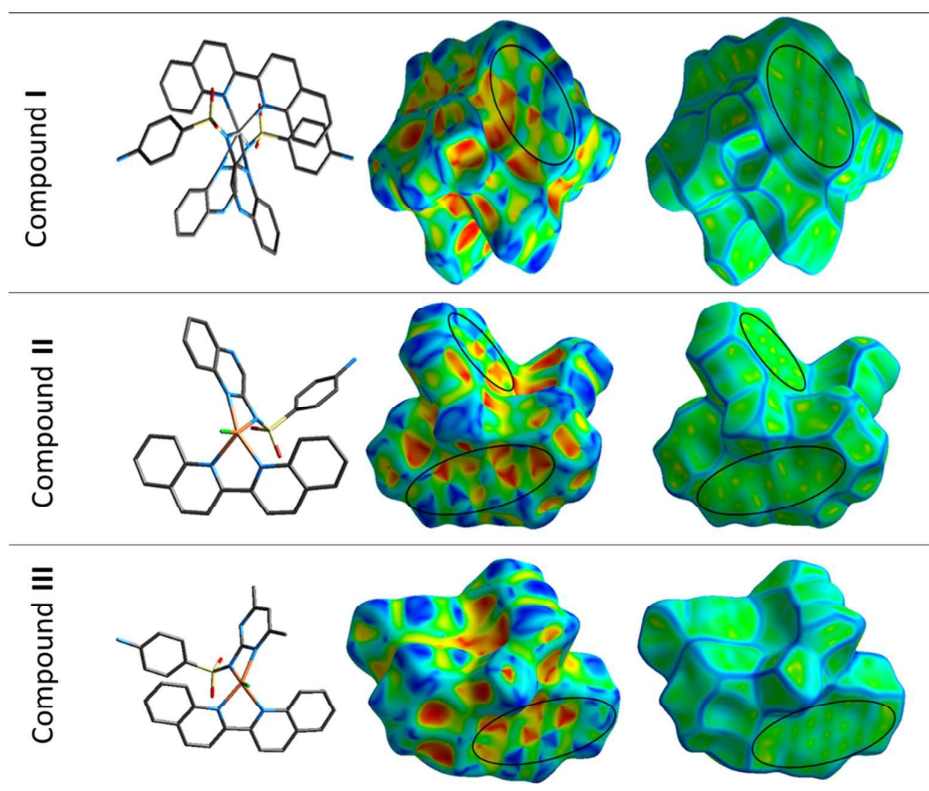
Figure 7. Hirshfeld surfaces mapped with *shape-index* and *curvedness* for the three complexes. The first column shows the orientation of the molecules in the surfaces. H-atoms were omitted for simplicity. Zones associated with π-π interactions are enclosed within a black oval.

2.3. Electronic Spectroscopy

UV-Vis and Diffuse Reflectance

In all the complexes, intraligand π-π* transitions are observed at a wavelength lower than 340 nm [37,38]. The nature of the d-d metal transitions has been studied by analyzing the UV-Vis (DMSO solutions) and the visible diffuse reflectance spectra (BaSO$_4$ solid matrix) of the complexes (Figure S3 in the ESI). For **I**, the V-DR spectrum shows bands at 610, 726 and 832 nm, in comparison with the values obtained from the UV-Vis spectrum (DMSO 40 mM solution) that displays bands at 610, 687 and 767 nm. These bands may tentatively be assigned to $^3A_{2g} \rightarrow {}^3T_{1g}(P)$, $^3A_{2g} \rightarrow {}^3T_{1g}$ and $^3A_{2g} \rightarrow {}^3T_{2g}$ transitions, respectively [39].

In the case of **II**, the V-DR spectrum shows two bands 478 and 545 nm, while in the UV-Vis spectrum (DMSO 10mM) these features are observed at 516 and 550 nm. For **III** the V-DR spectrum displays bands at 497 and 559 nm very close to those observed in the UV-Vis spectrum (DMSO 10 mM) at 451 and 558 nm. In both Cu(II) complexes, the bands may be assigned to the $^2B_1 \rightarrow {}^2E$ and $^2B1 \rightarrow {}^2B_2$ transitions. The observed features are in agreement with the spin allowed

d-d transitions of the d^8 six-coordinated Ni(II) [39] and the d^9 five-coordinated Cu(II) [40] complexes in both, solid and solution measurements.

Fluorescence Spectra

The solution fluorescence spectra of the complexes were investigated at room temperature, and the result is presented in Figure S4. The SQO and BQ ligands fluorescence spectra show bands at 420 nm (λ_{exc}= 310 nm) and 390 nm (λ_{exc}= 350 nm), respectively. Although the maximum of emission of the SQO ligand is observed when using excitation wavelength of 310 nm, the compound exhibits fluorescence at lower energy. In the SMT ligand spectrum, none transition has been observed, so in this ligand, the relaxation mechanism must follow a non-radiative pathway. The spectrum of complex **I** shows a band centered at 400 nm with a shoulder near 418 nm. These transitions can be assigned, to the BQ and the SQO intraligand fluorescence processes, respectively. The emission spectrum of compound **II,** shows two bands at 395 and 420 nm which can be assigned to the same processes as in **I**. The spectrum of complex **III** shows a broad band centered at 398 nm and can be assigned to biquinoline intraligand transitions. These assignments suggest that the compounds may be good candidates in blue-light-emitting materials, which may have potential applications in electronic devices.

2.4. Thermogravimetric behavior

TG curves of the complexes were measured in both, inert N_2 and oxidant O_2 atmospheres (see Figure S5 in the ESI). The TG curves (N_2 atmosphere) for all the complexes showed the incomplete decomposition up to 800 ºC while in oxidant atmosphere a complete decomposition was observed.

In all the complexes, the decomposition takes place in several overlapped steps. For that reason, it was not possible to determinate in detail the decomposition mechanisms nor the thermodynamic parameters of the steps.

For **I** the dehydration process occurs in the 40 - 90 ºC range, with the weight loss of 3.913 % consistent with the removal of two lattice water molecules (calculated 3.723 %). The corresponding process is observed with three endothermic peaks in the DT curve, as expected for the inequivalent water molecules and considering the disorder in one of them**.** At 270 °C started the continuous decomposition of the complex without formation of thermally stable intermediates up to 800 °C.

For **II**, a weight loss of 3.486 % between 15 and 80 ºC range associated with an endothermic peak is probably due to methanol solvation molecule (expected 4.660 %). The difference is probably attributed to the low temperature of the evolution of the methanol. The continuous decomposition of the complex occurs from 160 ºC involving exothermic processes. The anhydrous complex, **III,** was

thermally stable up to 150 °C when it started to decay involving exothermic peaks in DT curve. Further, the complex decomposed up to 800 °C. The DT curve for **III** showed a very exothermic peak at 640 ºC without mass loss; this fact could be explained by the intermediate formation of the reductant CO giving rise to Cu_2O product. Afterward, probably the Cu(I) oxide disproportionates to yield Cu(0) + CuO (no weight loss expected) [41].

However, TG curves measured in oxidant atmosphere showed the desolvation process and the complete decomposition of the complexes with a total oxidation to the metal oxides as observed in the FTIR spectra of the residues. Under this condition, no exothermic peak without a mass loss was observed in **III.** For all the complexes, the decomposition steps are associated with exothermic processes, except for the solvent loss of **I** and **II**. The remaining mass percentage for complexes **I, II** and **III** were 9.101, 10.252 and 11.852 %, respectively. From FTIR measurements the residues were identified as NiO for **I** and CuO for **II** and **III.**

2.5. Cytotoxic Effect

The bioinorganic medicinal chemistry is a constantly growing field, which it has been successful in offering therapeutic agents in the fight against different diseases that affect the global well-being. Some biological studies on ternary complexes of Cu(I), Ru(II) and Pd(II) including 2,2'-biquinoline (BQ) have been reported [42–44]. However, the effect of the free BQ ligand has not been informed yet. The three complexes, the free ligands and the parent salts were screened on both cell lines, MG-63 and A549. **I** was tested from 50 to 500 μM range and did not show a significant cytotoxic effect on the MG-63 cell line. The same effect was observed for the ligands, while the nickel chloride induced cell death in the upper range of concentrations (IC50 381.2 ± 9.6 μM). (see Figure 8a).

On the other hand, on the A549 cell line, the complex showed cytotoxic activity from 100 μM (P<0.0001). As can be seen in the Figure 8b the biquinoline ligand exhibited a higher effect than the complex, but the SQO did not show any effect in the whole range. At 200-500 μM range, there was no statistical difference (P>0.05) among the concentrations tested, which suggested a non-dose-related effect in this concentration range.

The IC_{50} values for the A549 cell line were 51.8 ± 8.4 μM, 112.3 ± 11.7 μM and 210.6 ± 12.8 μM and > 500 μM for the biquinoline, complex **I**, the Nickel ion and Sulfaquinoxaline, respectively. These results indicated that Biquinoline ligand had the highest effect on this cell line.
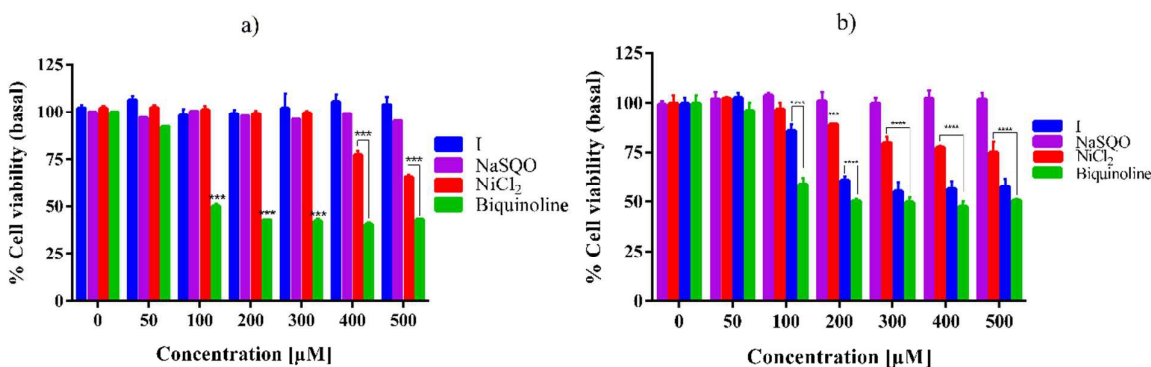
Figure 8. Effect of complex **I**, NaSQO and $NiCl_2$ on MG-63 human osteosarcoma cell viability evaluated by MTT (**a**). Effect of complex I, NaSQO $NiCl_2$, and biquinoline on A549 human lung carcinoma cell viability assessed by MTT (**b**). In both cases, cells were incubated in serum-free DMEM alone (control) or with different concentrations of the compounds at 37 °C for 24 h. The results are expressed as the percentage of the basal level and represent the mean ± SEM (n = 9). *** significant difference in comparison with the basal level (p < 0.001), **** significant difference as compared with the basal level (p < 0.0001).

On the other hand, complexes **II** and **III** showed a noticeable cytotoxic effect on MG-63 and A549 cell lines, as can be observed in the IC_{50} values included in Table 4.

Table 4. IC_{50} [μM] values on MG-63 and A549 cell lines for complexes I, II, III, the free ligands and metal salts.

Compound	IC_{50} MG-63	IC_{50} A549
I	> 500	112.3 ± 11.7
II	1.8 ± 0.3	1.6 ± 0.2
III	2.2 ± 0.2	1.9 ± 0.4
NaSQO	> 500	> 500
NaSMT	> 500	> 500
Biquinoline	> 10	51.8 ± 8.4
$NiCl_2$	381.2 ± 9.6	210.6 ± 12.8
$CuCl_2$	310.9 ± 4.5	> 100

As can be seen in Table 4, the effective concentrations of the complexes **II** and **III** as cytotoxic agents were below the action range of the ligands and the copper salt.

Complex **II** produced a statistically significant inhibitory effect on MG-63 cells from 1.5 μM (p<0.0001). This action extended to the full range of concentrations tested in a concentration related manner.

New Journal of Chemistry Accepted Manuscript

Complex **III** was less active in the low range of concentrations and the effect on MG-63 cells could be seen from 2.0 µM (p<0.0001). This compound also displayed a dose-dependent effect. (Figure 9a)

Likewise, complexes **II** and **III** also showed a deleterious effect on A549 lung cancer cells. Complex **II** induced cellular death at a lower concentration (1.5 µM, p<0.01) than complex **III** (2.0 µM, p<0.0001). (Figure 9b). Even though there were significant differences between complexes with mean values of 16 and 41 % for complex **II** and **III**, respectively (p<0.01) at lower concentrations, the complexes did not show a differential behavior at higher concentrations (p>0.05).

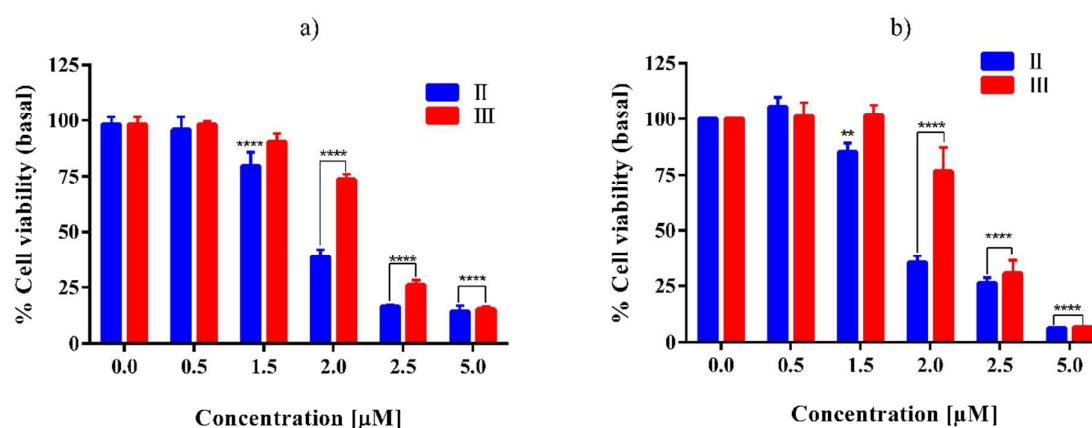**Figure 9.** Cytotoxic effect of complex **II** and **III** on MG-63 human osteosarcoma (**a**) and A549 human lung carcinoma cell lines (**b**), respectively evaluated by MTT. The results are expressed as the percentage of the basal level and represent the mean ± SEM (n = 9). ** significant difference in comparison with the basal level (p < 0.01), **** significant difference in relation to the basal level (p < 0.0001).

As we previously reported [45], copper complexes with different ligands like thiosemicarbazones, isoflavones, flavonoids and a variety of planar N-heterocycles had demonstrated to be effective in both in vitro and in vivo models. It is very known that the complexation of copper with active pharmaceuticals as ligands have demonstrated to be a potential source of anti-cancer drugs. Reports of this kind of complexes on osteosarcoma cell lines showed that induced not only cell death but also displayed a selective deleterious effect on tumor cell lines rather than normal phenotype cells. These findings are in agreement with our results [46,47].

Furthermore, it has been reported that quinoline derivatives enhance the cytotoxic effects against a wide range of cancer cells which includes ovarian, leukemia, breast, lung, and other cell lines [48–52].

In particular complexes with these ligands caused cellular death through different mechanisms such as induction of reactive oxygen species, DNA cleavage, cell cycle arrest and inhibition signaling pathways and different protein within the cell [53,54]. The observed deleterious effect could be related to the increased delocalization of pi-electrons caused by the chelating effect, which afterwards enhances the liposolubility of the compounds facilitating the permeation through membranes disrupting the cellular metabolic processes [55].

CONCLUSIONS

This study reports the synthesis and characterization of three monomeric ternary complexes of Ni(II) and Cu(II) with sulfanilamide derivatives (sulfaquinoxaline and sulfamethazine) and 2,2'-biquinoline as ligands. The spectroscopic and thermogravimetric properties resulted in good agreement with the X-ray crystallographic data. The stabilization of the crystal lattices due to the intermolecular interactions was studied using the Hirshfeld surface analysis. It was found that the intermolecular interactions of these compounds were dominated by Hydrogen bonds and $\pi \cdots \pi$ stacking interactions. All the complexes display fluorescence in the blue region of the spectrum so they could be widely exploited in many areas especially in light emitting devices.

The biological studies demonstrated that the antitumoral activity improves after complexation. Ni(II) complex did not cause a significant decrease in the cell viability. However, a substantial deleterious effect on A549 and MG-63 cancerous cells was observed in both Copper complexes since their IC50 value is lower than that of the free ligands and the $CuCl_2$ salt. These effects can trigger further in vivo experiments for studying their antineoplastic properties.

References

1   P. A. Ajibade, G. A. Kolawole and P. O. Brien, *Synth. React. Inorganic, Met. Nano-Metal Chem.*, 2007, **37:8**, 653–659.

2   A. M. Mansour and R. R. Mohamed, *RSC Adv.*, 2015, **5**, 5415–5423.

3   C. Villa-P?rez, J. F. Cadavid-Vargas, G. E. Cam?, F. Giannini, M. E. Chac?n Villalba, G. Echeverria, I. C. Ortega, G. C. Valencia-Uribe, S. B. Etcheverry and D. B. Soria, *Inorganica Chim. Acta*, 2016, **447**, 127–133.

4   W. C. Campbell, *J. Parasitol.*, 2008, **94**, 934–945.

5   J. B. Tommasino, F. N. R. Renaud, D. Luneau and G. Pilet, *Polyhedron*, 2011, **30**, 1663–1670.

6   J. H. B. Nunes, R. E. F. De Paiva, A. Cuin, A. M. Da Costa Ferreira, W. R. Lustri and P. P. Corbi, *J. Mol. Struct.*, 2016, **1112**, 14–20.

7   C. Villa-Pérez, I. Oyarzabal, G. A. Echeverría, G. C. Valencia-Uribe, J. M. Seco and D. B. Soria, *Eur. J. Inorg. Chem.*, 2016, **2016**, 4835–4841.

8   A. Bodoki, G. Alzuet, A. Hangan, L. Oprean, F. Estevan, A. Castiñeiras and J. Borrás, *Inorganica Chim. Acta*, 2010, **363**, 3139–3144.

9   F. Öztürk, İ. Bulut and A. Bulut, *Spectrochim. Acta Part A Mol. Biomol. Spectrosc.*, 2015, **138**, 891–899.

10 L. Gutiérrez, G. Alzuet, J. Borrás, A. Castiñeiras, A. Rodríguez-Fortea and E. Ruiz, *Inorg. Chem.*, 2001, **40**, 3089–3096.

11 İ. Bulut, F. Öztürk and A. Bulut, *Spectrochim. Acta Part A Mol. Biomol. Spectrosc.*, 2015, **138**, 138–145.

12 X.-H. Zhao, Y.-Y. Zhao, J. Zhang, J.-G. Pan and X. Li, *Acta Crystallogr. C.*, 2013, **69**, 1332–5.

13 J.-Y. Kang, S.-J. Huang, X.-H. Zhao, Y.-Y. Zhao and X. Li, *Chinese J. Inorg. Chem.*, 2015, **31**, 798–806.

14 Á. García-Raso, J. J. Fiol, S. Rigo, A. López-López, E. Molins, E. Espinosa, E. Borrás, G. Alzuet, J. Borrás and A. Castīeiras, *Polyhedron*, 2000, **19**, 991–1004.

15 G. M. G. Hossain, A. J. Amoroso, A. Banu and K. M. A. Malik, *Polyhedron*, 2007, **26**, 967–974.

16 I. Bulut and E. Biçer, *Russ. J. Electrochem.*, 2010, **46**, 62–71.

17 E. Elacqua, D. K. Bučar, R. F. Henry, G. G. Z. Zhang and L. R. MacGillivray, *Cryst. Growth Des.*, 2013, **13**, 393–403.

18 S. K. Wolff, D. J. Grimwood, J. J. McKinnon, M. J. Turner, D. Jyatilaka and M. A. Spackman, 2012.

19 M. A. Spackman and J. J. McKinnon, *Crystengcomm*, 2002, **4**, 378–392.

20 J. J. McKinnon, M. A. Spackman and A. S. Mitchell, *Acta Crystallogr. Sect. B Struct. Sci.*, 2004, **60**, 627–668.

21 G. Estiu, M. E. E. Chacón Villalba, G. E. E. Camí, G. a. a. Echeverria and D. B. B. Soria, *J. Mol. Struct.*, 2014, **1062**, 82–88.

22 G. Camí, E. Chacón Villalba, Y. Di Santi, P. Colinas, G. Estiu and D. B. Soria, *J. Mol. Struct.*, 2011, **995**, 72–77.

23 CrysAlis CCD, 2006.

24 G. M. Sheldrick, *Acta Crystallogr. A.*, 2008, **64**, 112–22.

25 G. M. Sheldrick, 1997.

26 G. M. Sheldrick, 1997.

27 M. J. Frisch, G. W. Trucks, H. B. Schlegel, G. E. Scuseria, M. A. Robb, J. R. Cheeseman, J. A. Montgomery, Jr., T. Vreven, K. N. Kudin, J. C. Burant, J. M. Millam, S. S. Iyengar, J. Tomasi, V. Barone, B. Mennucci, M. Cossi, G. Scalmani, N. Rega, G. A. Petersson, H. Nakatsuji, M. Hada, M.

Ehara, K. Toyota, R. Fukuda, J. Hasegawa, M. Ishida, T. Nakajima, Y. Honda, O. Kitao, H. Nakai, M. Klene, X. Li, J. E. Knox, H. P. Hratchian, J. B. Cross, V. Bakken, C. Adamo, J. Jaramillo, R. Gomperts, R. E. Stratmann, O. Yazyev, A. J. Austin, R. Cammi, C. Pomelli, J. W. Ochterski, P. Y. Ayala, K. Morokuma, G. A. Voth, P. Salvador, J. J. Dannenberg, V. G. Zakrzewski, S. Dapprich, A. D. Daniels, M. C. Strain, O. Farkas, D. K. Malick, A. D. Rabuck, K. Raghavachari, J. B. Foresman, J. V. Ortiz, Q. Cui, A. G. Baboul, S. Clifford, J. Cioslowski, B. B. Stefanov, G. Liu, A. Liashenko, P. Piskorz, I. Komaromi, R. L. Martin, D. J. Fox, T. Keith, M. A. Al-Laham, C. Y. Peng, A. Nanayakkara, M. Challacombe, P. M. W. Gill, B. Johnson, W. Chen, M. W. Wong, C. Gonzalez and J. A. Pople, 2004.

28   A. D. Becke, *J. Chem. Phys.*, 1993, **98**, 5648.

29   P. C. Hariharan and J. A. Pople, *Theor. chim. Acta*, 1973, **28**, 213–222.

30   P. J. Hay and W. R. Wadt, *J. Chem. Phys.*, 1985, **82**, 270.

31   W. R. Wadt and P. J. Hay, *J. Chem. Phys.*, 1985, **82**, 284.

32   P. J. Hay and W. R. Wadt, *J. Chem. Phys.*, 1985, **82**, 299.

33   T. Mosmann, *J. Immunol. Methods*, 1983, **65**, 55–63.

34   M. Llunell, D. Casanova, J. Cirera, J. . Bofill, P. Alemany, S. Alvarez, M. Pinsky and D. Avnir, 2005.

35   A. L. Spek, 2001.

36   K. Remya and C. H. Suresh, *Phys. Chem. Chem. Phys.*, 2015, **17**, 18380–18392.

37   A. M. Mansour, *J. Coord. Chem.*, 2013, **66**, 1118–1128.

38   K. K. Narang and J. K. Gupta, *Transit. Met. Chem.*, 1977, **2**, 83–86.

39   A. Majumder, G. M. Rosair, A. Mallick, N. Chattopadhyay and S. Mitra, *Polyhedron*, 2006, **25**, 1753–1762.

40   A. A. G. Tomlinson and B. J. Hathaway, *J. Chem. Soc. A Inorganic, Phys. Theor.*, 1968, 1905–1909.

41   C. H. Bamford and C. F. H. Tipper, *Chem. Kinet.*, 1980, **22**.

42   B. Peña, A. David, C. Pavani, M. S. Baptista, J. P. Pellois, C. Turro and K. R. Dunbar, *Organometallics*, 2014, **33**, 1100–1103.

43   J. Zhang, L. Li, L. Ma, F. Zhang, Z. Zhang and S. Wang, *Eur. J. Med. Chem.*, 2011, **46**, 5711–5716.

44   R. Starosta, A. Brzuszkiewicz, A. Bykowska, U. K. Komarnicka, B. Bażanów, M. Florek, Ł. Gadzała, N. Jackulak, J. Król and K. Marycz, *Polyhedron*, 2013, **50**, 481–489.

45   I. Leon, J. Cadavid-Vargas, A. Di Virgilio and S. Etcheverry, *Curr. Med. Chem.*, 2017, **24**, 112–148.

46   a. L. Di Virgilio, I. E. León, C. a. Franca, I. Henao, G. Tobón and S. B. Etcheverry, *Mol. Cell. Biochem.*, 2013, **376**, 53–61.

47   I. E. León, V. Porro, S. Astrada, M. G. Egusquiza, C. I. Cabello, M. Bollati-Fogolin and S. B. Etcheverry, *Chem. Biol. Interact.*, 2014, **222**, 87–96.

48   C. Santini, M. Pellei, V. Gandin, M. Porchia, F. Tisato and C. Marzano, *Chem. Rev.*, 2014, **114**, 815–862.

49   A. R. Martirosyan, R. Rahim-Bata, A. B. Freeman, C. D. Clarke, R. L. Howard and J. S. Strobl, *Biochem. Pharmacol.*, 2004, **68**, 1729–1738.

50 W. M. Motswainyana and P. A. Ajibade, *Adv. Chem.*, 2015, **2015**, 1–21.

51 N. Graf and S. J. Lippard, *Adv. Drug Deliv. Rev.*, 2012, 64, 993–1004.

52 S. Bhat, J. S. Shim, F. Zhang, C. R. Chong and J. O. Liu, *Org. Biomol. Chem.*, 2012, **10**, 2979–92.

53 V. Prachayasittikul, S. Prachayasittikul, S. Ruchirawat and V. Prachayasittikul, *Drug Des. Devel. Ther.*, 2013, **7**, 1157–1178.

54 V. Prachayasittikul, W. Chan-On, H. Nguyen Thi Bich, N. Songtawee, W. Suwanjang and S. Prachayasittikul, *Drug Des. Devel. Ther.*, 2015, **9**, 2033.

55 N. P. Priya, S. V. Arunachalam, N. Sathya, V. Chinnusamy and C. Jayabalakrishnan, *Transit. Met. Chem.*, 2009, **34**, 437–445.

New Journal of Chemistry Accepted Manuscript
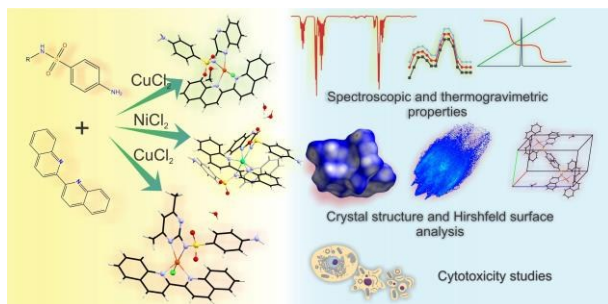
Three ternary complexes with Sulfaquinoxaline or Sulfamethazine have been synthesized; their structural, spectroscopic and biological properties have been studied.